RSC Advances

PAPER

View Article Online
View Journal | View Issue

Cite this: *RSC Adv.*, 2015, **5**, 59830

Energy transfer and luminescent properties of $Ca_8MgLu(PO_4)_7$:Tb^{3+}/Eu^{3+} as a green-to-red color tunable phosphor under NUV excitation†

Feiyan Xie,[ab] Junhao Li,[b] Zhiyue Dong,[b] Dawei Wen,[b] Jianxin Shi,*[b] Jing Yan[b] and Mingmei Wu*[b]

Received 10th May 2015
Accepted 3rd July 2015

DOI: 10.1039/c5ra08680a

www.rsc.org/advances

Two series of single-composition $Ca_8MgLu(PO_4)_7$:Tb^{3+} and $Ca_8MgTb(PO_4)_7$:Eu^{3+} phosphors were prepared by a high-temperature solid-state reaction technique, and their phase structures were characterized by powder X-ray diffraction (XRD). The excitation and emission spectra, and fluorescence decays were measured and discussed in detail. The results reveal that Tb^{3+} can efficiently transfer excitation energy to Eu^{3+} *via* its 4f states and therefore sensitizes Eu^{3+} emission under NUV excitation. By adjusting the ratio of Eu^{3+} and Tb^{3+}, we can tune the emission color of $Ca_8MgTb(PO_4)_7$:Eu^{3+} from green to yellow, orange and pure red. For $Ca_8MgTb_{0.1}(PO_4)_7$:0.9Eu^{3+}, the emission intensity at 150 °C is 87.44% of that at 25 °C, which makes it be a potential pure red phosphor for NUV LEDs.

Introduction

In the past decade, more and more interest has been focused on white light-emitting diodes (WLEDs), fabricated with a blue InGaN chip and yellow-emitting phosphor $Y_3Al_5O_{12}$:Ce^{3+}, due to their high brightness, long lifetime and environmental friendliness.[1–4] However, these blue InGaN-based WLEDs have some disadvantages such as low color rendering index (R_a) and unsatisfactory high color temperature because of the lack of red spectral component.[5,6] Moreover, the commonly used red phosphors for near ultraviolet (NUV) InGaN-based WLEDs are Y_2O_2S:Eu^{3+}, which shows some drawbacks such as a lower efficiency and shorter working lifetime, due to its instability.[7] Therefore, there is an urgent need to develop novel and stable red phosphors with intense emission upon NUV excitation.

In the search for red-emitting phosphors with high efficiency and proper CIE chromaticity coordinates, the Eu^{3+} activated phosphors are primarily considered for the reason that Eu^{3+} ions can emit red light with an excellent color purity. However, the low oscillator strength of 4f → 4f absorption transitions such as $^7F_0$ → $^5D_4$, $^5L_7$ and $^5D_3$ or the narrow line width of $^7F_0$ → $^5L_4$ transition (~395 nm) for Eu^{3+} leads to a weak absorption in the NUV region or a mismatch absorption with NUV from LED chip.[8] Thus, it is necessary to find sensitizers for Eu^{3+} luminescence.

With the development of the chip technology, the emission of InGaN LED chip extends to NUV region (350–400 nm) and the commercially available NUV LED chip from 375 to 380 nm is more and more common.[9–11] Therefore, the sensitization effect of Tb^{3+} ions for red emitting ions, Eu^{3+}, has attracted great attention.[12–14] Tb^{3+} ions not only enhance the emission of Eu^{3+} but also broaden the absorption region due to the existence of more impurity energy levels introduced by Tb^{3+}. It is clear that Tb^{3+} acts as a good sensitizer to enhance the luminescence efficiency of Eu^{3+} ions in $K_2Ln(PO_4)(WO_4)$,[15] $Ba_3La(PO_4)_3$,[16] $SrMg_2La_2W_2O_{12}$,[17] $TbBO_3$:Eu^{3+},[18] $TbPO_4$:Eu^{3+},[19] and $KCaY(PO_4)_2$:Tb^{3+},Eu^{3+} (ref. 20) phosphors. Moreover, the emitting color of the phosphors can be tuned by adjusting the ratio of Tb^{3+} and Eu^{3+} ions. The realization of tunable multicolor emission under a single excitation wavelength in phosphors is beneficial for potential application in display device.

Phosphates are excellent hosts for luminescent materials because of their facile synthesis condition, good chemical stability and low cost. The $Ca_8MgLn(PO_4)_7$ (Ln = Y, La, Gd or Lu) compound has whitlockite-like structure with space group *R3c* as β-$Ca_3(PO_4)_2$. As a typical of phosphate, β-$Ca_3(PO_4)_2$ has six metal sites (M1–M6) in the crystal lattice. M1 and M2 sites are coordinated by eight oxygen atoms, M3 and M5 sites are surrounded by nine and six oxygen atoms, M4 site surrounded by nine oxygen atoms is 50% occupied by Ca^{2+} ions, and M6 site is vacant.[21–23] The special structure suggests that the lattice can accommodate other cations with similar radii and charges without significant changes in the structural framework. Moreover, the hexagonal crystal structure of $Ca_8MgLu(PO_4)_7$ also favors the energy transfer from Tb^{3+} to Eu^{3+}. $Ca_8MgLn(PO_4)_7$:Eu^{2+},Mn^{2+} (Ln = La or Y)

[a]*Department of Chemical Engineering, Huizhou University, Huizhou, 516007, P. R. China*

[b]*Key Laboratory of Bioinorganic and Synthetic Chemistry of Ministry of Education, School of Chemistry and Chemical Engineering, Sun Yat-Sen University, Guangzhou 510275, P. R. China. E-mail: cessjx@mail.sysu.edu.cn; ceswmm@mail.sysu.edu.cn; Fax: +86 20 8411 2245; Tel: +86 20 8411 2830*

† Electronic supplementary information (ESI) available. See DOI: 10.1039/c5ra08680a

phosphors have been reported for WLEDs due to their outstanding luminescence properties.[21] $Ca_8MgLn(PO_4)_7:Eu^{3+}$ (Ln = La, Gd or Y) phosphors have been synthesized and focused on the site-selective spectroscopy of Eu^{3+}.[24] To the best of our knowledge, the luminescence properties of $Ca_8MgLu(PO_4)_7:Tb^{3+}$ and $Ca_8MgTb(PO_4)_7:Eu^{3+}$ have not been reported. In this study, we report the synthesis and characterization of an emitting color tunable phosphor, $Ca_8MgTb(PO_4)_7:Eu^{3+}$. The mechanism of energy transfer between Tb^{3+} and Eu^{3+} in the phosphor was investigated, and the results show that the thermally stable luminescence of $Ca_8MgTb_{0.1}(PO_4)_7:0.9Eu^{3+}$ could serve as a potential pure red phosphor for NUV LEDs.

Experimental

Two series of phosphors with the compositions of $Ca_8MgLu_{1-x}(PO_4)_7:xTb^{3+}$ and $Ca_8MgTb_{1-y}(PO_4)_7:yEu^{3+}$ were synthesized by a high temperature solid-state reaction method. The raw materials were $CaCO_3$ (A. R.), $NH_4H_2PO_4$ (A. R.), $(MgCO_3)_4\cdot Mg(OH)_2\cdot 5H_2O$ (A. R.), Lu_2O_3 (99.99%), Tb_4O_7 (99.99%) and Eu_2O_3 (99.99%), respectively. The raw materials with a stoichiometric ratio were mixed by grinding in an agate mortar. After mixing and grinding, the mixtures were put into crucibles and subsequently heated at 1200 °C in a chamber furnace for 3.0 h in air. Finally, the as-synthesized samples were cooled down slowly to room temperature and then ground into powder for measuring.

The structure of the samples was examined with a Rigaku D-max 2200 X-ray diffraction system with a Cu Kα radiation at 30 kV and 30 mA. The photoluminescence (PL), PL excitation (PLE) spectra and the decay curves at room temperature were measured by FLS 920-combined Time Resolved and Steady State Fluorescence Spectrometer (Edinburgh Instruments) equipped with a 450 W Xe lamp, a 60 W μF flash lamp. The temperature-dependent PL spectra were obtained on the same instrument with a temperature-controller.

Results and discussion

Crystal structures of $Ca_8MgLu(PO_4)_7:Tb^{3+}$ and $Ca_8MgTb(PO_4)_7:Eu^{3+}$

Fig. 1 shows the powder XRD patterns for $Ca_8MgLu(PO_4)_7$, $Ca_8MgLu_{0.3}(PO_4)_7:0.7Tb^{3+}$, $Ca_8MgTb(PO_4)_7$, $Ca_8MgTb_{0.1}(PO_4)_7:0.9Eu^{3+}$, and the reference diffraction lines based on the JCPDS card with no. 46-0803. The results of XRD analysis confirm that the compounds were obtained as single phase. No extra diffraction peaks related to the starting materials were observed. All the diffraction peaks of the samples can be indexed to the standard data of $Ca_8MgLu(PO_4)_7$ (JCPDS card no. 46-0803). The crystal structure of $Ca_8MgLu(PO_4)_7$ is hexagonal with space group of $R3c$, and cell parameters of $a = b = 10.337$ Å, $c = 36.915$ Å, $V = 3416.2$ Å^3, and $Z = 6$. The crystal structure of $Ca_8MgLu(PO_4)_7$ and coordination condition of Ca^{2+} is presented in Fig. 2. There are six metal sites (M1–M6) in this crystal. M1 and M2 sites are coordinated by eight oxygen atoms, M3 and M5 sites are surrounded by nine and six oxygen atoms, M4 site surrounded by nine oxygen atoms is 50% occupied by Ca^{2+} ions, and M6 site is vacant. For $Ca_8MgLu(PO_4)_7$, Ca^{2+} and Lu^{3+} mainly occupy M1, M2 and M3, while Mg^{2+} occupies M5 site.[21] It was found that as Lu^{3+} is substituted by the larger Tb^{3+} or Eu^{3+} ion, the entire diffraction profile shifts slightly towards a lower 2θ angle.

Luminescence properties of $Ca_8MgLu(PO_4)_7:Tb^{3+}$ and $Ca_8MgTb(PO_4)_7:Eu^{3+}$

The excitation and emission spectra of $Ca_8MgLu_{0.1}(PO_4)_7:0.9Tb^{3+}$ phosphor are presented in Fig. 3a and b, respectively. This excitation spectrum is taken at an emission wavelength of 543 nm, which reveals a series of spectral bands in the range from 280 nm to 400 nm. The f–f transitions are ascribed to the transitions of Tb^{3+} ions from the ground state of $^7F_6$ to the higher energy states of $^5H_3$ (285 nm), $^5H_6$ (303 nm), $^5D_0$ (319 nm), $^5G_2$ (341 nm), $^5D_2$ (351 nm), $^5L_{10}$ (368 nm), and $^5G_6$ (378 nm), respectively.[25] The emission spectrum of the sample covers the region from 480 to 700 nm as excited at 378 nm. This spectrum consists of the characteristic transitions of Tb^{3+}, $^5D_4 \rightarrow {}^7F_6$ (488 nm), $^5D_4 \rightarrow {}^7F_5$ (543 nm), $^5D_4 \rightarrow {}^7F_4$ (585 nm) and $^5D_4 \rightarrow {}^7F_3$ (620 nm).[26] Among these characteristic peaks, the emission of the $^5D_4 \rightarrow {}^7F_5$ transition at 543 nm is predominant and is predicted by the large values of the reduced matrix elements at $J = 5$ and the Judd–Ofelt theory.[27]

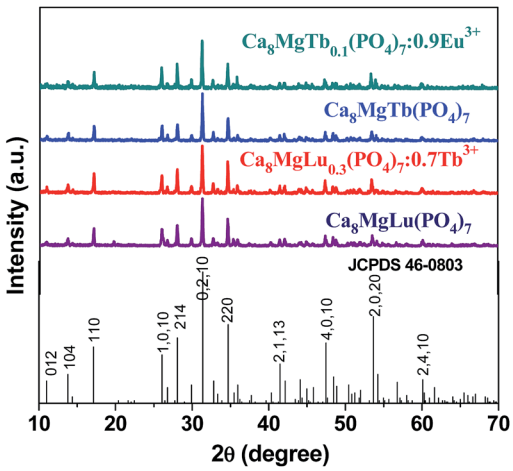

Fig. 1 Powder XRD patterns for $Ca_8MgLu(PO_4)_7$, $Ca_8MgLu_{0.3}(PO_4)_7:0.7Tb^{3+}$, $Ca_8MgTb(PO_4)_7$, $Ca_8MgTb_{0.1}(PO_4)_7:0.9Eu^{3+}$, and the standard data of $Ca_8MgLu(PO_4)_7$ (JCPDS card no. 46-0803).

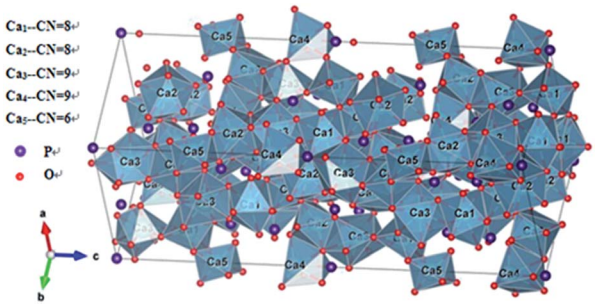

Fig. 2 The crystal structure of $Ca_8MgLu(PO_4)_7$ and coordination condition of Ca^{2+}.

The emission intensities of Tb^{3+} as a function of the doping concentrations and decay curves of Tb^{3+} in $Ca_8MgLu_{1-x}(PO_4)_7$:xTb^{3+} are given in Fig. 3c and d, respectively. It can be seen that luminescence intensities of Tb^{3+} are enhanced with the increase of their Tb^{3+} concentrations in Fig. 3c. The decay curves of Tb^{3+} are nearly overlapped one another at different Tb^{3+} concentrations as shown in Fig. 3d. The decay time for all $Ca_8MgLu_{1-x}(PO_4)_7$:xTb^{3+} (x = 0.1–1.0) samples at room temperature were measured to be ~2.1 ms. These observations confirm that the concentration quenching of Tb^{3+} does not occur in $Ca_8MgLu(PO_4)_7$ host, which can be explained by the crystal structure of the host matrix. $Ca_8MgLu(PO_4)_7$ has a typical whitlockite structure with a space group of $R3c$. In the structure of $Ca_8MgLu(PO_4)_7$, the cell in the hexagonal setting can accommodate a high concentration of cations with various valence states and various sizes due to six distinct Ca^{2+} sites, with coordination number ranging from 6 to 9 and various Ca–O distances.[23] In the structure, sites M1–M3 and M5 are fully occupied, but the site M4 is only half occupied and the M6 site is vacant. Hence, we consider that this special structure is an important factor for no concentration quenching phenomenon.

Fig. 4 illustrates the PLE and PL spectra of the typical $Ca_8MgTb_{0.7}(PO_4)_7$:$0.3Eu^{3+}$. The PLE spectrum monitored at 612 nm of Eu^{3+} consists of 4f–4f excitation transitions of Tb^{3+}. These results give a direct evidence of sensitizing Eu^{3+} by Tb^{3+}. $^5D_2$, $^5L_{10}$ and $^5G_6$ of Tb^{3+} are very close to each other. Meanwhile, $^5D_4$, $^5G_2$ and $^5L_7$ of Eu^{3+} are close to each other. Eu^{3+} can make full use of those energy levels to form a combinatorial absorption, resulting from energy transfer process of $Tb^{3+} \rightarrow Eu^{3+}$. Thus, the absorption region of Eu^{3+} can be broadened (see Fig. S1. ESI†). The excitation spectra which irradiated wavelength of 544 nm were identical to that of Tb^{3+} singly doped phosphor, which shows $Ca_8MgTb(PO_4)_7$ can be used as green and red double-color-emitting phosphors in NUV-pumped WLEDs. On the other hand, the emission peaks of Eu^{3+}, Tb^{3+} co-doped phosphor under 378 nm excitation were observed at 612 nm and 543 nm, attributed to the Eu^{3+} and Tb^{3+} ions, respectively. Therefore, the relative intensities of these two emissions can be varied by adjusting the concentrations of the two activators through the principle of energy transfer.[10]

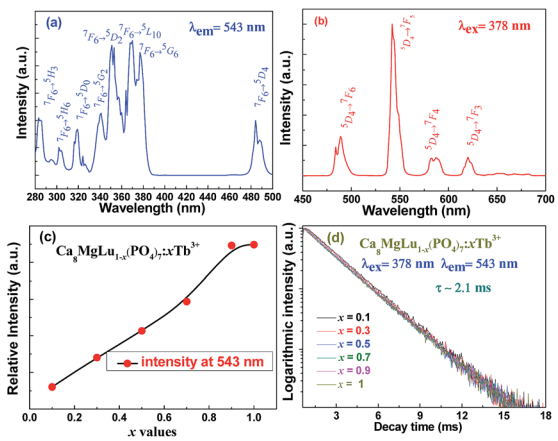

Fig. 3 (a) Excitation and (b) emission spectra of $Ca_8MgLu_{0.1}(PO_4)_7$:$0.9Tb^{3+}$, (c) the dependence of emission intensities on Tb^{3+} contents and (d) decay curves of $Ca_8MgLu_{1-x}(PO_4)_7$:xTb^{3+} (x = 0.1–1.0).

Color-tunable emission of $Ca_8MgTb(PO_4)_7$:Eu^{3+} under NUV excitation

Fig. 5 shows the emission spectra of $Ca_8MgTb_{1-y}(PO_4)_7$:yEu^{3+} with different Eu^{3+} contents under 378 nm excitation. In $Ca_8MgTb(PO_4)_7$ sample with no Eu^{3+}-doping, the characteristic emissions of Tb^{3+} are observed. With the doping of Eu^{3+} (y = 0.1), besides the emission of Tb^{3+}, we can also observe the emission of Eu^{3+}. With the increase of Eu^{3+} concentration, the luminescence of Tb^{3+} begins to decrease and that of Eu^{3+} increases, which are the results of the enhancing probability of energy transfer from Tb^{3+} to Eu^{3+}. Therefore, $Ca_8MgTb_{1-y}(PO_4)_7$:yEu^{3+} (y = 0–0.7) samples show a tunable emission from green to red, depending on the ratio of Tb^{3+} to Eu^{3+}. As shown in the CIE chromaticity diagram of Fig. 6 and Table 1, the CIE chromaticity coordinates of the corresponding samples are shifting from (0.331, 0.592) to (0.644, 0.352). More importantly, the coordinate of the red emission sample $Ca_8MgTb_{0.1}(PO_4)_7$:$0.9Eu^{3+}$ is (0.644, 0.352), which is very close to the National Television System Committee (NTSC) standard for red subpixels (0.67, 0.33).[28] The digital photos of $Ca_8MgTb(PO_4)_7$:Eu^{3+} in Fig. 5 also support the spectral results. $Ca_8MgTb(PO_4)_7$:Eu^{3+} can be used as green-red double color phosphors for NUV-based WLEDs.

Energy transfer mechanism of $Tb^{3+} \rightarrow Eu^{3+}$ in $Ca_8MgTb(PO_4)_7$:Eu^{3+}

Luminescence decay time measurements are performed to further analyze the energy transfer phenomenon. Fluorescence decays of samples $Ca_8MgTb_{1-y}(PO_4)_7$:yEu^{3+} with different doping concentration (y = 0–0.9) at room temperature are shown in Fig. 7a. A single-exponential decay process was observed with different y values in $Ca_8MgTb_{1-y}(PO_4)_7$:yEu^{3+}, the curves were well fitted by the following equation,[25]

$$I_t = I_0 \exp(-t/\tau) \quad (1)$$

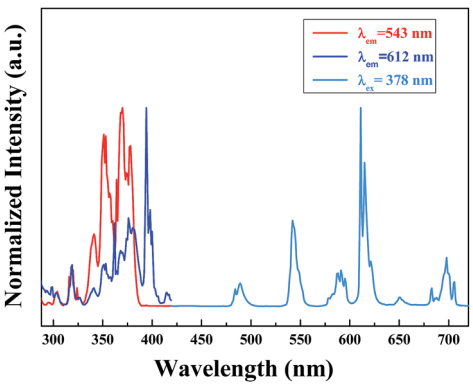

Fig. 4 PLE and PL spectra of $Ca_8MgTb_{0.7}(PO_4)_7$:$0.3Eu^{3+}$ phosphor.

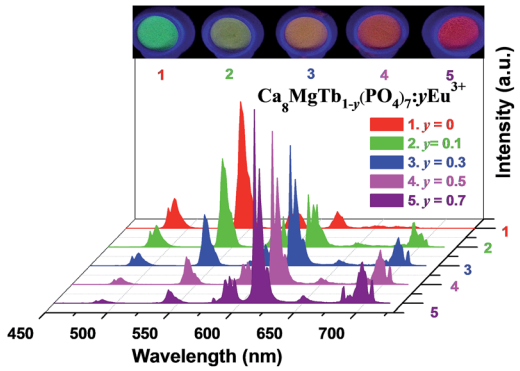

Fig. 5 PL spectra (λ_{ex} = 378 nm) and luminescence photographs (λ_{ex} = 365 nm) of $Ca_8MgTb_{1-y}(PO_4)_7$:yEu^{3+} (y = 0, 0.1, 0.3, 0.5, 0.7).

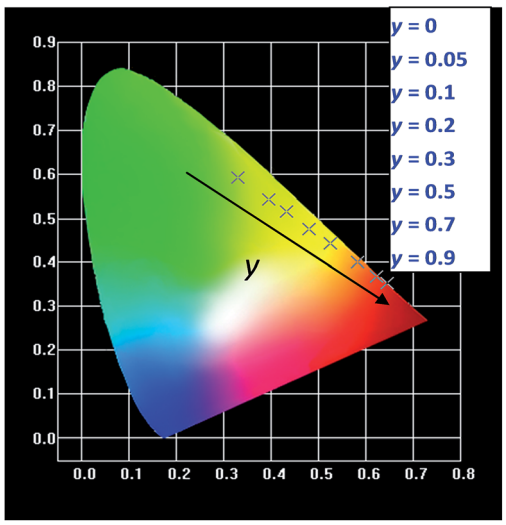

Fig. 6 CIE chromaticity diagram for $Ca_8MgTb_{1-y}(PO_4)_7$:yEu^{3+} (y = 0–0.9) under 378 nm excitation.

Table 1 Comparison of the CIE chromaticity coordinates for $Ca_8MgTb_{1-y}(PO_4)_7$:yEu^{3+} excited at 378 nm

Sample no.	%Eu^{3+}	CIE coordinates (x, y)
1	0	(0.331, 0.592)
2	5	(0.395, 0.542)
3	10	(0.432, 0.514)
4	20	(0.480, 0.476)
5	30	(0.524, 0.443)
6	50	(0.582, 0.399)
7	70	(0.623, 0.368)
8	90	(0.644, 0.352)

where I_t and I_0 are the luminescence intensities at time t and t = 0, respectively, and τ is the decay time. The values of τ were calculated to be about 2.05, 1.92, 1.75, 1.49, 1.32, 1.14, 1.00 and 0.98 ms for $Ca_8MgTb_{1-y}(PO_4)_7$:yEu^{3+} with y = 0.0, 0.05, 0.1, 0.2, 0.3, 0.5, 0.7 and 0.9, respectively, as shown in Fig. 7b. It can be observed that the decay time of Tb^{3+} ions decreases with increasing the contents of Eu^{3+}, due to the energy transfer from Tb^{3+} to Eu^{3+}. Eqn (2) can be used to estimate the energy transfer probability ($P_{Tb\rightarrow Eu}$) from Tb^{3+} to Eu^{3+},[29]

$$P_{Tb\rightarrow Eu} = \frac{1}{\tau} - \frac{1}{\tau_0} \quad (2)$$

where τ_0 and τ are the corresponding lifetimes of the donor Tb^{3+} in the absence and presence of the acceptor Eu^{3+} for the same donor concentration, respectively. The energy transfer efficiency ($\eta_{Tb\rightarrow Eu}$) is also evaluated from eqn (3),

$$\eta_{Tb\rightarrow Eu} = 1 - \frac{\tau}{\tau_0} \quad (3)$$

According to the above eqn (2) and (3), the values of $P_{Tb\rightarrow Eu}$ and $\eta_{Tb\rightarrow Eu}$ can be calculated in Table 2 and Fig. 8, respectively. The results indicate that the energy transfer efficiency from Tb^{3+} to Eu^{3+} is effective and strongly depends on the doping concentration of Eu^{3+} in $Ca_8MgTb(PO_4)_7$ host. Clearly, it is known from Fig. 8 that the energy transfer efficiency from Tb^{3+} to Eu^{3+} increases gradually with the increase in Eu^{3+} concentration.

Fig. 9 illustrates the decay curves of $Ca_8MgTb_{1-y}(PO_4)_7$:yEu^{3+} (λ_{ex} = 378 nm, λ_{em} = 612 nm). Two different processes can be observed for Eu^{3+} emission, decay process and build-up process. In the build-up process, the energy absorbed by the

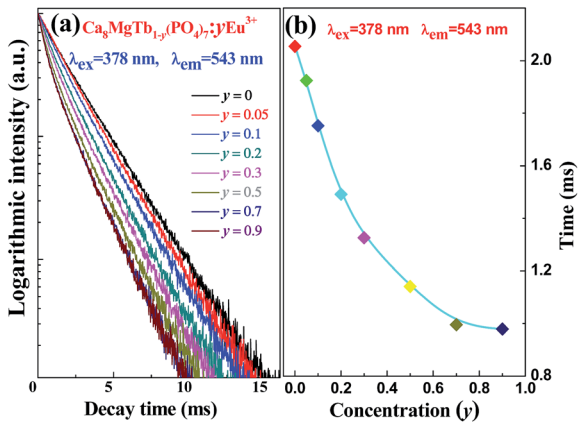

Fig. 7 (a) Decay curves and (b) fluorescence lifetimes of Tb^{3+} under 378 nm excitation as a function of y values in $Ca_8MgTb_{1-y}(PO_4)_7$:yEu^{3+} (y = 0–0.9).

Table 2 Energy transfer probabilities and efficiencies of Tb^{3+} → Eu^{3+} in $Ca_8MgTb_{1-y}(PO_4)_7$:yEu^{3+}

%Eu^{3+}	Decay time (ms)	$P_{Tb\rightarrow Eu}$ (ms^{-1})	$\eta_{Tb\rightarrow Eu}$
0	2.05	0	0
5	1.92	0.033	0.06
10	1.75	0.084	0.14
20	1.49	0.183	0.27
30	1.32	0.270	0.36
40	1.22	0.332	0.40
50	1.14	0.389	0.44
60	1.05	0.465	0.49
70	1.00	0.512	0.51
80	0.99	0.522	0.52
90	0.98	0.533	0.52

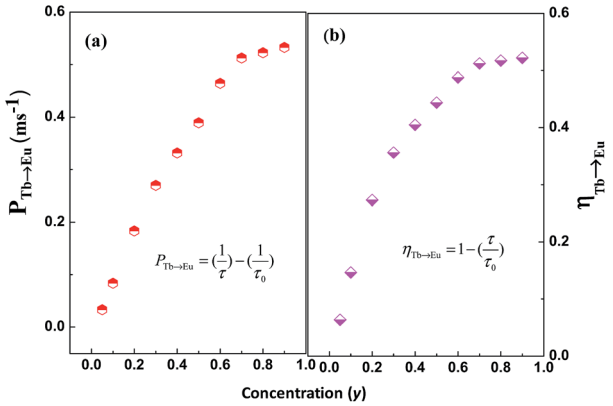

Fig. 8 Dependence of (a) energy transfer probability $P_{Tb\to Eu}$ and (b) efficiency $\eta_{Tb\to Eu}$ on Eu^{3+} concentration (y = 0.05, 0.1, 0.2, 0.3, 0.4, 0.5, 0.6, 0.7, 0.8, 0.9) in $Ca_8MgTb_{1-y}(PO_4)_7$:yEu^{3+}.

$^7F_6 \rightarrow {}^5G_6$ transition in Tb^{3+} ions is transferred to Eu^{3+} ions. The build-up process is significantly influenced by the content of Eu^{3+}. As shown in Fig. 9a, the build-up process becomes faster and faster with increasing the content of Eu^{3+} ions, which indicates that the energy transfer process from Tb^{3+} to Eu^{3+} becomes more efficient with the increase of Eu^{3+}. When the $Ca_8MgTb_{1-y}(PO_4)_7$:yEu^{3+} samples are excited by 378 nm, the rate equations for the population densities in the $^5D_4$ level of Tb^{3+} ion and $^5D_0$ of Eu^{3+} ion can be expressed as follows[25,30]

$$\frac{dN_{Tb}}{dt} = -\frac{N_{Tb}}{\tau_{Tb}} - K_{Tb-Eu}N_{Tb} \quad (4)$$

$$\frac{dN_{Eu}}{dt} = -\frac{N_{Eu}}{\tau_{Eu}} + K_{Tb-Eu}N_{Tb} \quad (5)$$

where the N_{Tb} and N_{Eu} are the population intensities of the $^5D_4$ level of Tb^{3+} and $^5D_0$ of Eu^{3+}, respectively. K_{Tb-Eu} is the non-radiative energy transfer rate from the $^5D_4$ state of Tb^{3+} to $^5D_0$ of Eu^{3+}. Then the fluorescence intensity I_t of Eu^{3+} ions at 612 nm under 378 nm excitation can be given as following,

$$I(t) = N_{Eu}(t) = \frac{K_{Tb-Eu}N_{Tb}}{\frac{1}{\tau_{Eu}} - \frac{1}{\tau_{Tb}}}\left[\exp\left(-\frac{t}{\tau_{Tb}}\right) - \exp\left(-\frac{t}{\tau_{Eu}}\right)\right] \quad (6)$$

Using the measured values of τ_{Tb} and τ_{Eu}, the theoretical curves for the $Ca_8MgTb_{1-y}(PO_4)_7$:yEu^{3+} samples are obtained as presented in Fig. 9b, which show two processes for Eu^{3+} emission, being similar to the measured curves. That is to say, the theoretical curves are consistent with the experimental ones.

The energy transfer scheme of Tb^{3+}–Eu^{3+} in $Ca_8MgTb(PO_4)_7$ host is shown in Fig. 10. The Tb^{3+} ions can be excited from the ground state ($^7F_6$) to the excited states by UV light, and then relax to the lowest excited state $^5D_4$ through multiphonon relaxation, then radiatively return to ground states (^7F_J). When co-doped with Eu^{3+}, the energy from $^5D_4$–^7F_J transitions of Tb^{3+} will be transferred to Eu^{3+} through cross-relaxation, which will relax to the $^5D_0$ (Eu^{3+}) level, where the orange-red emission ($^5D_0 \rightarrow {}^7F_J$) takes place. Because the $^5D_4 \rightarrow {}^7F_J$ emission of Tb^{3+}

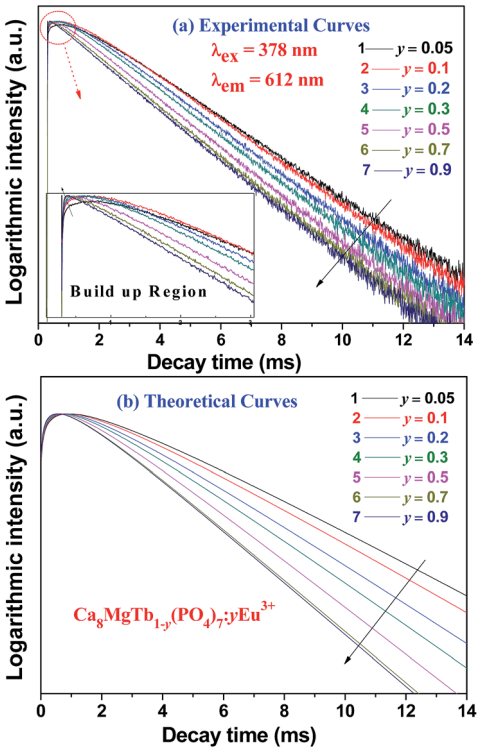

Fig. 9 (a) Experimental decay curves and (b) the corresponding theoretical curves for $Ca_8MgTb_{1-y}(PO_4)_7$:yEu^{3+}.

is effectively overlapped with the $^7F_{0,1} \rightarrow {}^5D_{0,1,2}$ absorption of Eu^{3+}, the energy transfer from Tb^{3+} to Eu^{3+} is efficient.[18] Exchange interactions and multipolar interactions are two main aspects of the resonant energy-transfer mechanism. The energy transfer between the Tb^{3+} and Eu^{3+} ions mainly takes place by exchange interactions.[8,18,19]

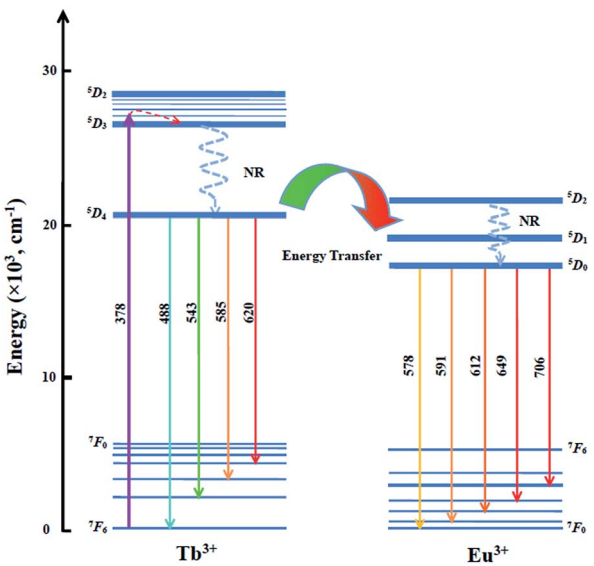

Fig. 10 Schematic energy–level diagram of Tb^{3+} and Eu^{3+} in $Ca_8MgTb(PO_4)_7$ and energy transfer from Tb^{3+} to Eu^{3+}.

The distance between Tb^{3+} and Eu^{3+} ions can be estimated by using the equation pointed out by Blasse,[31]

$$R_c \approx 2\left[\frac{3V}{4\pi x_c N}\right]^{\frac{1}{3}} \quad (7)$$

where R_c corresponds to the mean separation between the nearest $Tb^{3+}$and Eu^{3+} ions at x_c, V is the volume of the unit cell, N is the number of available sites for the dopant in the unit cell and x_c is the concentration. In this case, V is estimated to be 3447.1 Å^3, x_c is 1 and N is 6 due to 6 divalent metal sites in the unit cell.[21] The distance R_{Tb-Eu} is calculated to be 10.31 Å. This value is much longer than 5 Å, the critical distance of the exchange interaction.[8,32] So the concentration quenching of Tb^{3+} does not occur in $Ca_8MgLu(PO_4)_7$ host, which is consistent with the previous conclusion obtained from the point of crystal structure.

Thermally stable luminescence of $Ca_8MgTb(PO_4)_7:Eu^{3+}$

The thermal quenching property is one of the important technological parameters for phosphors used in solid-state lighting because it has a considerable influence on the light output and color rendering index. The temperature dependence of the integrated emission intensity of $Ca_8MgTb_{0.1}(PO_4)_7:0.9Eu^{3+}$ excited with 378 nm is illustrated in Fig. 11a upon heating the phosphor in a temperature range from 25 to 200 °C. When the temperature is increased up to 150 °C and 200 °C, the emission integrated intensity is 87.44% and 79.18% of that at 25 °C. The results are better than those of some red phosphors, such as $NaGd(WO_4)_2:Tm^{3+},Dy^{3+},Eu^{3+}$, 51.60% at 200 °C,[33] and $LaMgAl_{11}O_{19}:Sm^{3+},Eu^{3+}$, 56% at 150 °C.[34] The CIE chromaticity coordinates of $Ca_8MgTb_{0.1}(PO_4)_7:0.9Eu^{3+}$ sample at different temperatures are also shown (see Table S1 ESI†), which show that the phosphor has a good color stability. Therefore, $Ca_8MgTb(PO_4)_7:Eu^{3+}$ phosphor has an excellent thermal stability and could be potential for high-powered LED applications. In order to understand the temperature dependence of emission intensity and to determine the activation energy for thermal quenching, the Arrhenius equation was used to fit the thermal quenching data of the $Ca_8MgTb_{0.1}(PO_4)_7:0.9Eu^{3+}$ phosphor,[35]

$$I = \frac{I_0}{1 + A\exp\left(-\frac{\Delta E}{kT}\right)} \quad (8)$$

where I_0 is the initial emission intensity, I is the intensity at different temperatures, ΔE is activation energy of thermal quenching, A is a constant for a certain host and k is Boltzmann constant (8.617×10^{-5} eV). Eqn (8) can be revised as,

$$-\frac{\Delta E}{kT} + \ln A = \ln\left(\frac{I_0}{I} - 1\right) \quad (9)$$

As shown in Fig. 11b, the experimentally calculated activation energy ΔE was 0.15 eV for $Ca_8MgTb_{0.1}(PO_4)_7:0.9Eu^{3+}$.

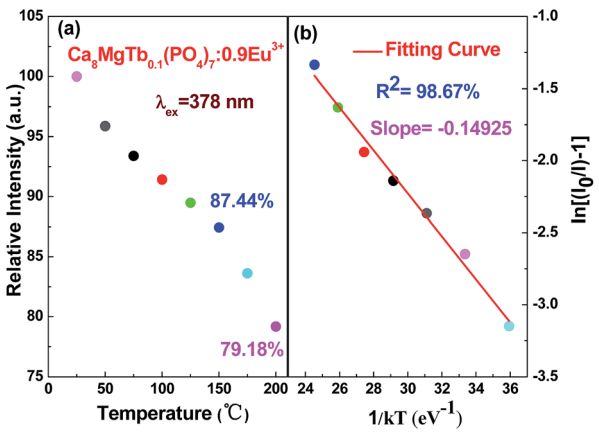

Fig. 11 (a) Temperature dependence of the emission integrated intensity of $Ca_8MgTb_{0.1}(PO_4)_7:0.9Eu^{3+}$ and (b) the Arrhenius fitting result.

Conclusions

In summary, $Ca_8MgLu(PO_4)_7:Tb^{3+}$ and $Ca_8MgTb(PO_4)_7:Eu^{3+}$ phosphors were prepared using a high-temperature solid-state reaction technique. The energy transfer process of $Tb^{3+} \rightarrow Eu^{3+}$ has been investigated by the photoluminescence emission and excitation spectra, the decay curves, and the effect of the ratio of Tb^{3+} to Eu^{3+}. It is demonstrated that Tb^{3+} can efficiently sensitize the luminescence of Eu^{3+} under NUV excitation due to effective energy transfer from Tb^{3+} to Eu^{3+}, and the energy transfer efficiency increases with increasing the concentration of Eu^{3+}. $Ca_8MgTb_{1-y}(PO_4)_7:yEu^{3+}$ (y = 0–0.9) phosphors exhibit bright emission under 378 nm excitation and the emission color can be tunable from green, to yellowish-green and red region. Moreover, the temperature-dependence of luminescence shows that $Ca_8MgTb(PO_4)_7:Eu^{3+}$ phosphor has an excellent thermal stability. These results indicate that $Ca_8MgTb(PO_4)_7:Eu^{3+}$ can be promising as a potential candidate for the application in NUV-based WLEDs.

Acknowledgements

This work was financially supported by grants from the Joint Funds of the National Natural Science Foundation of China (NNSFC) and Guangdong Province (No. U1301242), NNSFC (21271190), Research Fund for the Doctoral Program of Higher Education of China (RFDP) (No. 20130171130001), the Government of Guangdong Province for Industrial Applications of Rare Earth Photoluminescence Materials (2012B091000026 and 2013A090100010), the Natural Science Foundation of Guangdong Province (No. 9151027501000047 and S2012020011113), and the Natural Science Foundation of Huizhou university (No. hzuxl201301).

References

1 Y. Liu, Y. Wang, L. Wang, Y.-Y. Gu, S.-H. Yu, Z.-G. Lu and R. Sun, *RSC Adv.*, 2014, **4**, 4754.
2 Q. Y. Zhang and Z. G. Xia, *RSC Adv.*, 2014, **4**, 53237.

3 D. W. Wen, G. H. Yang, H. Yang, J. X. Shi, M. L. Gong and M. M. Wu, *Mater. Lett.*, 2014, **125**, 63.
4 D. W. Wen, H. Yang, G. H. Yang, J. X. Shi, M. M. Wu and Q. Su, *J. Solid State Chem.*, 2014, **213**, 65.
5 C. H. Huang, P. J. Wu, J. F. Lee and T. M. Chen, *J. Mater. Chem.*, 2011, **21**, 10489.
6 S. Hur, H. J. Song, H. S. Roh, D. W. Kim and K. S. Hong, *Ceram. Int.*, 2013, **39**, 9791.
7 K. Deng, T. Gong, Y. H. Chen, C. K. Duan and M. Yin, *Opt. Lett.*, 2011, **36**, 4470.
8 X. Zhang, L. Zhou, Q. Pang, J. Shi and M. Gong, *J. Phys. Chem. C*, 2014, **118**, 7591.
9 G. V. Lokeswara Reddy, L. Rama Moorthy, T. Chengaiah and B. C. Jamalaiah, *Ceram. Int.*, 2014, **40**, 3399.
10 J. Zhou and Z. G. Xia, *J. Mater. Chem. C*, 2014, **2**, 6978.
11 Y. Kojima, M. Numazawa and T. Umegaki, *J. Lumin.*, 2012, **132**, 2648.
12 D. W. Wen, J. X. Shi, M. M. Wu and Q. Su, *ACS Appl. Mater. Interfaces*, 2014, **6**, 10792.
13 X. J. Li, Y. Zhang, D. L. Geng, J. S. Lian, G. Zhang, Z. Y. Hou and J. Lin, *J. Mater. Chem. C*, 2014, **2**, 9924.
14 Z. H. Xu, C. X. Li, G. G. Li, R. T. Chai, C. Peng, D. M. Yang and J. Lin, *J. Phys. Chem. C*, 2010, **114**, 2573.
15 D. W. Wen, J. J. Feng, J. H. Li, J. X. Shi, M. M. Wu and Q. Su, *J. Mater. Chem. C*, 2015, **3**, 2107.
16 C. H. Zhang, H. B. Liang, S. Zhang, C. M. Liu, D. J. Hou, L. Zhou, G. B. Zhang and J. Y. Shi, *J. Phys. Chem. C*, 2012, **116**, 15932.
17 K. Pavani, J. Suresh Kumar and L. Rama Moorthy, *J. Alloys Compd.*, 2014, **586**, 722.
18 J. Yang, C. M. Zhang, C. X. Li, Y. N. Yu and J. Lin, *Inorg. Chem.*, 2008, **47**, 7262.
19 X. G. Zhang, L. Y. Zhou, J. X. Shi and M. L. Gong, *Mater. Lett.*, 2014, **137**, 32.
20 W. H. Di, X. J. Wang, P. F. Zhu and B. J. Chen, *J. Solid State Chem.*, 2007, **180**, 467.
21 D. W. Wen, Z. Y. Dong, J. X. Shi, M. L. Gong and M. M. Wu, *ECS J. Solid State Sci. Technol.*, 2013, **2**, 178.
22 R. A. Benhamou, A. Bessière, G. Wallez, B. Viana, M. Elaatmani, M. Daoud and A. Zegzouti, *J. Solid State Chem.*, 2009, **182**, 2319.
23 A. Bessière, R. A. Benhamou, G. Wallez, A. Lecointre and B. Viana, *Acta Mater.*, 2012, **60**, 6641.
24 Y. L. Huang, C. F. Jiang, Y. G. Cao, L. Shi and H. J. Seo, *Mater. Res. Bull.*, 2009, **44**, 793.
25 C. M. Liu, D. J. Hou, J. Yan, L. Zhou, X. J. Kuang, H. B. Liang, Y. Huang, B. B. Zhang and Y. Tao, *J. Phys. Chem. C*, 2014, **118**, 3220.
26 H. Yu, W. W. Zi, S. Lan, S. C. Gan, H. F. Zou, X. C. Xu and G. Y. Hong, *Opt. Laser Technol.*, 2012, **44**, 2306.
27 G. S. Ofelt, *J. Chem. Phys.*, 1962, **37**, 511.
28 G. Y. Dong, H. X. Ma, Y. F. Liu, Z. P. Yang and Q. B. Liu, *Opt. Commun.*, 2012, **285**, 4097.
29 Y. C. Li, Y. H. Chang, Y. S. Chang, Y. J. Lin and C. H. Laing, *J. Phys. Chem. C*, 2007, **111**, 10682.
30 J. Zhong, H. Liang, Q. Su, J. Zhou, Y. Huang, Z. Gao, Y. Tao and J. Wang, *Appl. Phys. B*, 2010, **98**, 139.
31 G. Blasse, *Philips Res. Rep.*, 1969, **24**, 131.
32 D. L. Dexter and J. A. Schulman, *J. Chem. Phys.*, 1954, **22**, 1063.
33 Y. Liu, G. X. Liu, J. X. Wang, X. T. Dong and W. S. Yu, *Inorg. Chem.*, 2014, **53**, 11457.
34 X. Min, Z. H. Huang, M. H. Fang, Y. G. Liu, C. Tang and X. W. Wu, *Inorg. Chem.*, 2014, **53**, 6060.
35 Z. G. Xia, X. M. Wang, Y. X. Wang, L. B. Liao and X. P. Jing, *Inorg. Chem.*, 2011, **50**, 10134.

